ACCEPTED VERSION

Yadong Zhou, An Deng

Modelling combined electroosmosis-vacuum-surcharge preloading consolidation considering large-scale deformation

Computers and Geotechnics, 2019; 109:46-57

Final publication at http://dx.doi.org/10.1016/j.compgeo.2019.01.013

Modelling combined electroosmosis–vacuum–surcharge preloading consolidation considering large-scale deformation

Yadong Zhou[a] and An Deng[*b]

[a] School of Civil Engineering
Tianjin Chengjian University
Tianjin 300384, China

*Corresponding author
[b]School of Civil, Environmental and Mining Engineering
The University of Adelaide
Adelaide SA 5000, Australia

E-mail addresses: zyd476300@126.com (Yadong Zhou). an.deng@adelaide.edu.au (An Deng).

Abstract: A numerical model, EC3, which was developed to simulate soil consolidation arising from the combined electroosmosis–vacuum–surcharge preloading processes, is presented. The EC3 model improves on its predecessor, model EC2, through incorporating the additional preloading element of vacuum and simulating the consolidation in three-dimensional (3D) space. In EC3, the 3D consolidation was simulated in polar coordinates, which allows for concurrent flows in the radial and vertical directions. The rates of the flows were formulated using the finite difference method. This method enables the model to approximate large-deformation consolidation where the deformation has yielded nonlinear changes in soil properties and nonlinear Darcy fluid flow. The performance of the model was validated against laboratory test results, and the model was applied to example problems in order to optimise the combined consolidation processes. The optimisation results suggested that the combined electroosmosis–vacuum–surcharge preloading process outperforms any two element combination processes with respect to the attained final soil layer settlement when the input parameters remain the same. The presence of a smear zone decreases the consolidation rate but increases the final settlement. The less permeable the smear zone is, the less the attained consolidation rate in the soil layer.

Keywords: Large-scale deformation consolidation; electrokinetic; finite difference; permeability

1 Introduction

Although vacuum preloading is identified as a workable solution to aid in soil consolidation [1], the results of vacuum preloading are satisfactory for silty soils, but not for clayey soils or other fine deposits [2]. In the clayey soil conditions, a portion of the clay drifts under the applied vacuum pressure and forms clogs in the proximity of the drains [3, 4]. Though the clay is thin, this clogging severely restricts the vacuum pressure to a limited zone of influence and bars the efficient flow of water [5]. This concern does not noticeably occur in soils that are consolidated under surcharge preloading. However, this process is time-dependent and, for clayey soils, is less viable for meeting goals when time is a factor; the timing issue escalates the process of deciding where to consolidate a thick layer. Thick layers can occur in cases of estuarine reclamation, sewage slurry and mine waste dumps, where the deposits range from metres to tens of metres. To accelerate the consolidation, one solution is to combine the process of electroosmosis with the vacuum–surcharge preloading method, enabling a tri-element consolidation solution. The electroosmosis component has shown to be effective in driving a stream of water through a clogging smear zone or a less permeable area [6, 7], and the performance complements the other two elements, as reported in various applications [8-10].

The setup of the electroosmosis–vacuum–surcharge preloading process is illustrated in Figure 1. Added to the vacuum–surcharge preloading system is an array of electrodes that are installed in the soil layer of interest. The cathodes coincide with the prefabricated vertical drains (PVD), and the anodes are installed between the drains. Although the anodes and cathodes can line up, as discussed in Deng and Zhou [11], to facilitate their installations, the electrodes are often laid out in a triangular pattern, as illustrated in Figure 1 (b), enabling a radial flow mode and efficient drainage. For a cell of radial flow, the zone of influence and its profile view, which includes the soil layer conditions, is provided in Figure 2. The soil layer, which is H_0 in thickness, is subjected to a surcharge load, q_0, vacuum pressure, $-p$, and an electric field with voltage, V. The zone of influence is subdivided into three sections: the native soil, the smear zone, and the drain, all in the radial direction. The three sections, in the form of concentric cylinders, correspond to the radii r_e, r_s, and r_w.

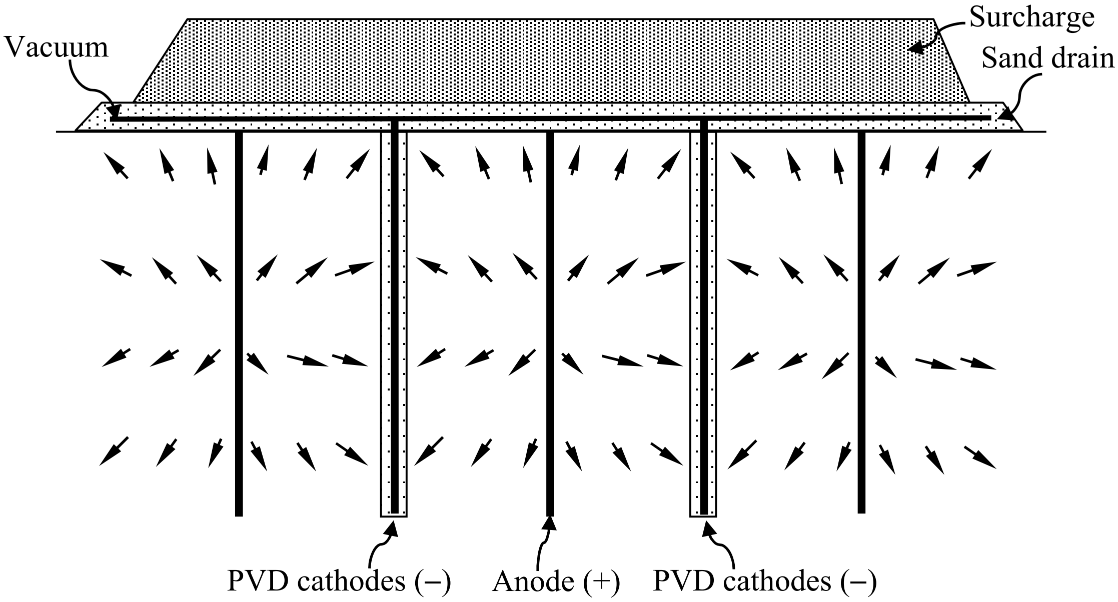

(a)

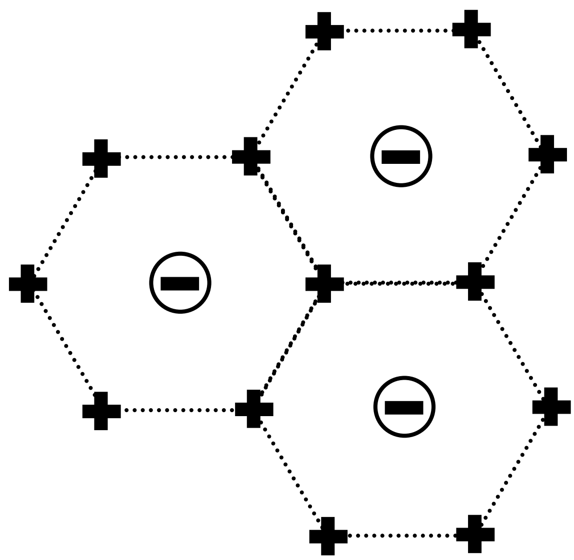

(b)

Figure 1 Schematic of electroosmosis−vacuum−surcharge preloading installation: (a) profile,

(b) Triangular layout of PVDs–electrodes.

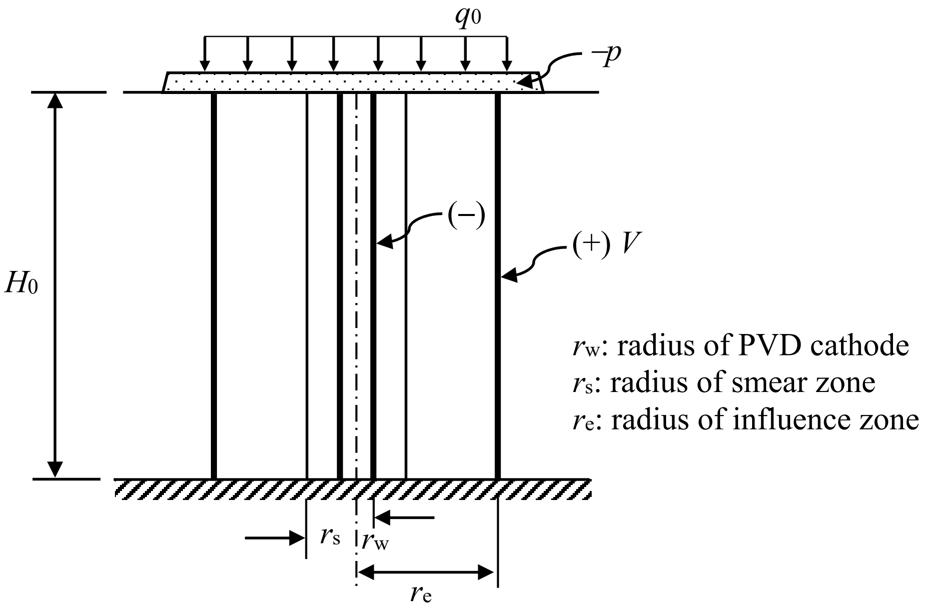

Figure 2 A cell of soil layer subjected to electroosmosis–vacuum–surcharge preloading.

To model the consolidation occurring in the cell, a point of departure is the model developed by Wan and Mitchell [12]. Their model was developed in terms of a schematic similar to the one presented in Figure 2. However, they only considered the electroosmosis–surcharge preloading process. To simplify the process, they sealed the top and bottom boundaries and restricted the hydraulic flow to the horizontal direction. To eliminate this restriction, two-dimensional (2D) models, e.g., Shang [13] and Hu *et al.* [14], were developed. With the advance in vacuum preloading techniques, additional models were developed either for vacuum–surcharge preloading (e.g., Kianfar *et al.* [15], Vu and Yang [16], Wu and Hu [17]) or electroosmosis–vacuum–surcharge preloading (e.g., Deng and Zhang [18], Wu and Hu [19]). These models, in essence, used or referred to Terzaghi's consolidation theory and were proven to be suitable for linear Darcy fluid flow stands and small-deformation conditions, e.g., shallow or thin layers, or small load increments where soil properties (e.g., the permeability k) are assumed constant throughout the process. When the soil layer is thick and large deformation has occurred, as per Townsend and Mcvay [20], the soil properties vary in the course of consolidation, which invalidates the constant-property assumption.

To consider the varying soil properties, the finite element method was used to simulate one-dimensional (1D) (e.g., Feldkamp [21]) and 2D consolidation problems (e.g., Yuan and Hicks [22]). The results obtained from the finite element method are not accurate enough when large deformation occurs due to mesh distortion or boundary variation. To avoid these limitations, the finite difference method was used to develop a 1D model, EC1 [7], and a 2D model, EC2 [11]. As per Fox *et al.* [23], the finite difference method offers greater versatility with regard to initial conditions, boundary conditions, time step increments, body deformations, and soil heterogeneity than models based on material coordinates. This means that the material space and the time space are examined separately and coupled to gain better simulation accuracy. Deng and Zhou [11] confirmed the advantages and showcased it in their simulation study [6]. Their studies, however, were applied to the square layout of vertical drains and are not applicable to the triangular layout pattern. The radial–vertical consolidation arising from the triangular layout pattern requires further examination.

In this study, model EC3 was developed as a tool used to simulate consolidation of a soil layer that is subjected to a combined electroosmosis–vacuum–surcharge preloading process. As with models EC1 and EC2, model EC3 uses the finite difference method and formulates the streams of flow that occur in the soil layer. The objective of this work is to solve the 3D consolidation simulations of a soil layer where large-deformation settlement occurs and nonlinear Darcy fluid flow arises from the combined three preloading elements. As in Fox *et al.* [23], EC3 uses polar coordinates to formulate the streams. The capability of model EC3 was validated against laboratory test results. The model was then applied to example problems to examine the performance of this combined preloading process with a goal of optimisation. The optimisation will address two aspects: *i*) the consolidation efficiency of the combined preloading process, and *ii*) the effect of the smear zone on the consolidation results. As with models EC1 and EC2, model EC3 assumes the following conditions: *i*) no chemical change in the soil, *ii*) no evolution of gas at the electrodes, and *iii*) fully saturated soil during consolidation. Meanwhile, at each time step, the consolidation is small, and the small-strain conditions stand. In addition, EC3 assumes a constant vacuum pressure throughout the layer. This assumption is suboptimal but helps simplify the process of vacuum preloading and isolate the effects of soil types on vacuum pressure distributions.

2 Model Description

2.1 Geometry

The cell in Figure 2 is adapted to the geometry shown in Figure 3 (a). As per definitions in Fox *et al.* [23], a saturated, homogeneous soil layer associated with a single drain is treated as an idealised two-phase material in which the solid particles and the pore fluid are incompressible. The soil layer of initial thickness H_0 and radius $r_e = d_e/2$ has radial symmetry. At t=0, the drain has a length of penetration given by $L_d \leq H_0$ and an equivalent radius of $r_w = d_w/2$. A smear zone surrounding the drain has an equivalent radius of $r_s = d_s/2$. The anodes (+) sit on the outermost periphery, and the cathode (–) sits on the rim of the drain. The soil layer is subjected to an initial vertical effective stress q_0 at the top and has completed the corresponding primary consolidation. Only vertical compression takes place. Mass continuity is assumed throughout the consolidation process.

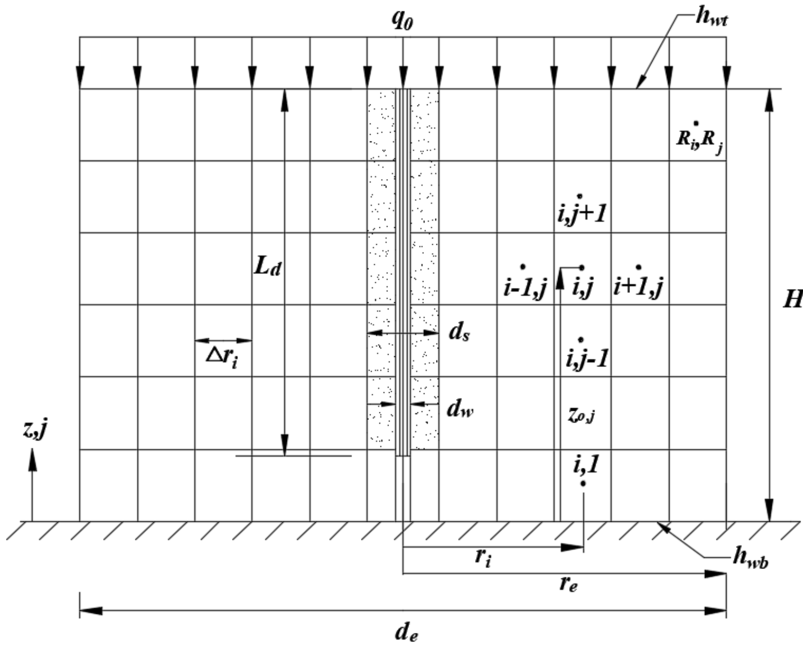

(a)

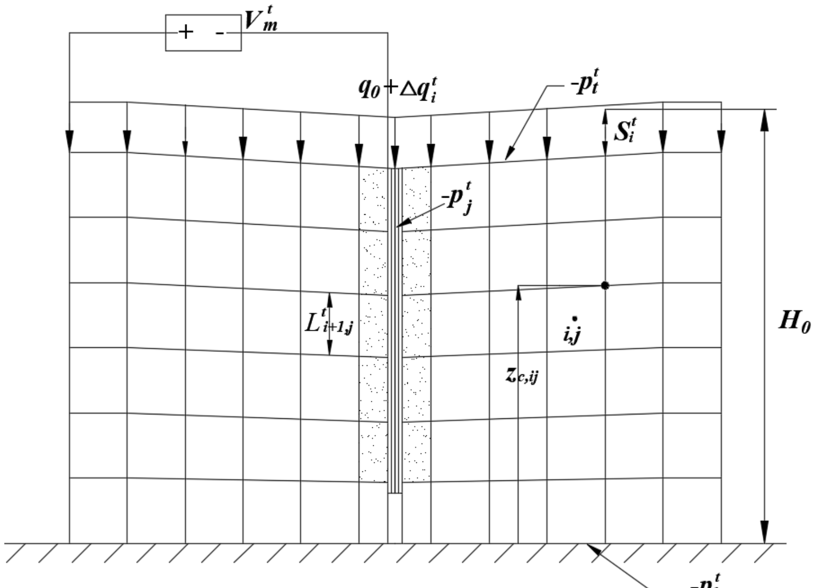

(b)

Figure 3 EC3 geometry for a soil layer H_0 that is subjected to a voltage V_{m}^t, vacuum load $-p^t$, and surcharge increment Δq^t: (a) initial configuration ($t = 0$), and (b) configuration after layer deformation S^t ($t > 0$).

An Eulerian coordinate system, (r, z), is defined as positive outward from the centre of the drain and positive upward (against gravity) from a fixed datum plane coincident with the bottom of the soil layer. The soil layer is sliced equally in the radial direction (from the cathode to the anode) into R_i elements and, in the vertical direction (in an upward sense), into R_j elements, forming a mesh of $R_\mathrm{i} \times R_\mathrm{j}$ elements. Element ij, where i= 1, 2, …, R_i and j = 1, 2, …, R_j, has a rectangular cross section of width $\Delta r_i = r_\mathrm{e}/R_\mathrm{i}$, an initial height of $L_0 = H_0/R_\mathrm{j}$, a central node located at initial elevation $z_{0,j}$ a radial coordinate r_i, and an initial void ratio $e_{0,ij}$. Each node contains consolidation data for the corresponding element, e.g., the pore water pressure, settlement, and flow rate. The top and bottom boundaries of the soil layer can be specified as drained or closed. Where drained, the heads are specified as h_wt and h_wb. The vertical drain is assumed to have negligible resistance to flow, and the boundary at the anode is specified as closed.

At t = 0, a time-dependent combined load with voltage V_m^t, vertical effective stress increment Δq_i^t, and vacuum load $-p_j^t$ on the drain, $-p_\mathrm{t}^t$ on the top, and $-p_\mathrm{b}^t$ on the bottom, are applied to the soil layer. At $t > 0$, the soil layer deforms as shown in Figure 3 (b). Then, the average height L_{ij}^t and elevation z_{ij}^t of element ij are updated as

$$L_{ij}^t = \frac{z_{\mathrm{c},(i-1)j}^t - z_{\mathrm{c},(i-1)(j-1)}^t + z_{\mathrm{c},ij}^t - z_{\mathrm{c},i(j-1)}^t}{2} \tag{1}$$

$$z_{ij}^t = \frac{z_{\mathrm{c},(i-1)j}^t + z_{\mathrm{c},(i-1)(j-1)}^t + z_{\mathrm{c},ij}^t + z_{\mathrm{c},i(j-1)}^t}{4} \tag{2}$$

where $z_{\mathrm{c},ij}^t$ is the elevation of the upper-outer corner of element ij at time t and is expressed as

$$z_{\mathrm{c},ij}^t = z_{\mathrm{c},(i-1)j}^t + z_{\mathrm{c},i(j-1)}^t - z_{\mathrm{c},(i-1)(j-1)}^t + \frac{3\Delta r_i\left(A_{ij}^t - \pi\left(z_{\mathrm{c},(i-1)j}^t - z_{\mathrm{c},(i-1)(j-1)}^t\right)\left(r_\mathrm{b}^2 - r_\mathrm{a}^2\right)\right)}{\pi\left(r_\mathrm{a}^3 - 3r_\mathrm{a}r_\mathrm{b}^2 + 2r_\mathrm{b}^3\right)} \tag{3}$$

where A_{ij}^t is the volume of element ij at time t, $r_\mathrm{a} = r_i - (\Delta r_i/2)$, $r_\mathrm{b} = r_i + (\Delta r_i/2)$, and the node radial coordinate $r_i = (i - 0.5)\Delta r_i$.

2.2 Constitutive relationships

The constitutive relationships for the compressible soil layer are presented in Figure 4. The void ratio e is monotonically decreasing with the vertical effective stress σ'. The hydraulic conductivity k_h (and electroosmotic conductivity k_e) is monotonically increasing with the void ratio e. The relationships are usually nonlinear, which agrees with structured fissures or voids in most native, clayey soils. The relationships for k_h and k_e are independent and determined in terms of corresponding laboratory tests. Based on Deng and Zhou [11], the relationships can be determined as:

$$\Delta e / \Delta \log k_{\mathrm{h}} = C_{\mathrm{k}} \tag{4}$$

$$k_{\mathrm{e}} = k_{\mathrm{e0}} \left(\frac{(1+e_0)e}{e_0(1+e)} \right)^a \tag{5}$$

where parameters C_k and a, the initial void ratio e_0, and the initial electroosmotic conductivity k_{e0} are determined based on test results.

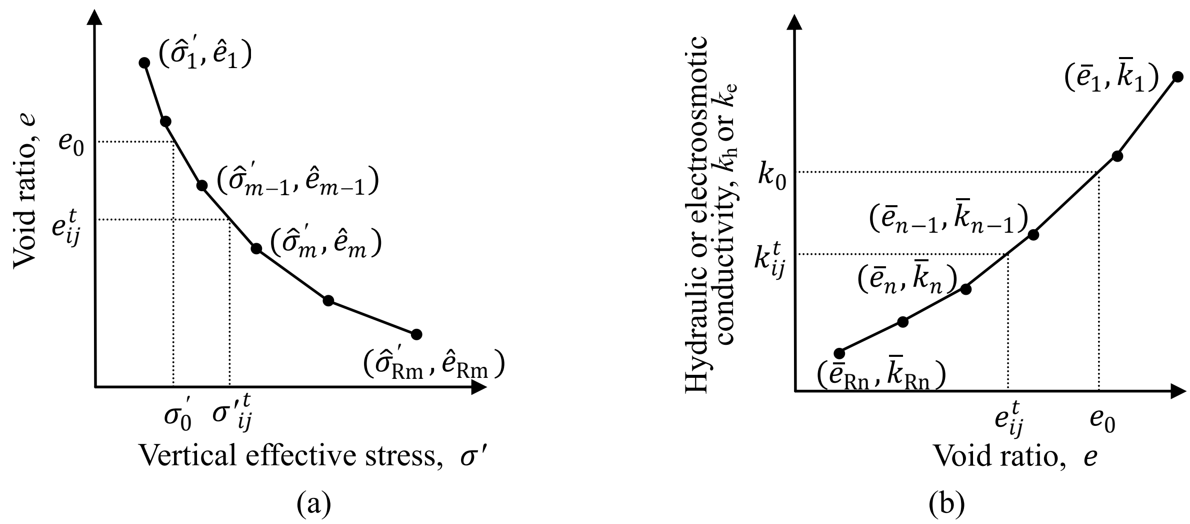

Figure 4 Soil constitutive relationships: (a) compressibility obtained from R_m loads, and (b) permeability obtained from R_n void ratios (adapted from [23]).

2.3 Total stress, effective stress, and pore pressure

The vertical total stress at the node of each element in Figure 3 is computed from the applied overburden stress and the self-weight of the compressible soil layer. At $t > 0$, the total stress at node ij, σ^t_{ij}, is calculated as

$$\sigma^t_{ij} = \left(h^t_{\mathrm{w},i} - \frac{z^t_{\mathrm{c},(i-1)R_\mathrm{j}} + z^t_{\mathrm{c},iR_\mathrm{j}}}{2} \right) \gamma_\mathrm{w} + q_0 + \Delta q^t_i + \frac{A^t_{ij}\gamma^t_{ij}}{4\pi r_i \Delta r_i} + \sum_{k=j+1}^{R_\mathrm{j}} \frac{A^t_{ik}\gamma^t_{ik}}{2\pi r_i \Delta r} \tag{6}$$

where γ^t_{ij} is the saturated unit weight of element ij and is expressed as

$$\gamma^t_{ij} = \frac{G_\mathrm{s} + e^t_{ij}}{1 + e^t_{ij}} \gamma_\mathrm{w} \tag{7}$$

where e^t_{ij} is the void ratio of element ij at time t, G_s is the specific gravity of the soil solids, and γ_w is the unit weight of water. In consolidation, G_s and γ_w remain unchanged for the soil layer, and e^t_{ij} is constant within each element over any given time increment.

According to the compressibility curve (Figure 4 (a)) and e^t_{ij} of element ij at time t, the vertical effective stress σ'^t_{ij} at node ij is interpolated as

$$\sigma'^t_{ij} = \hat{\sigma}'_{m-1} + \frac{\hat{e}_{m-1} - \hat{e}^t_{ij}}{a^t_{\mathrm{v},m-1}} \tag{8}$$

where $a^t_{\mathrm{v},m-1}$ is the coefficient of compressibility and is calculated as the slope (absolute value) of the linear segment of the compressibility curve between points $(\hat{\sigma}'_{m-1}, \hat{e}_{m-1})$ and $(\hat{\sigma}'_m, \hat{e}_m)$. The pore pressure at node ij, u^t_{ij}, is the difference between the total and effective stresses:

$$u^t_{ij} = \sigma^t_{ij} - \sigma'^t_{ij} \tag{9}$$

2.4 Electrical resistivity and electric potential

Electrical resistivity is a function of void ratio, and, as discussed in Deng and Zhou [11], the electrical resistivity for element *ij* is expressed as

$$\rho_{ij}^{t} = \frac{1}{\frac{1}{\rho_{\mathrm{s}}}\frac{1}{1+e_{ij}^{t}} + \frac{1}{\rho_{\mathrm{w}}}\frac{e_{ij}^{t}}{1+e_{ij}^{t}}} \tag{10}$$

where ρ_{s} and ρ_{w} are the electrical resistivities of solid particles and pore water, respectively. In terms of the model geometry (Figure 3), the electrical resistance of element *ij* is expressed as

$$R_{ij}^{t} = \frac{\rho_{ij}^{t}\Delta r_{i}}{2\pi r_{i} L_{ij}^{t}} \tag{11}$$

A voltage V_{m}^{t} is applied between the anodes and the cathode. The electric potential at node *ij*, V_{ij}^{t}, is determined as

$$V_{ij}^{t} = V_{\mathrm{m}}^{t}\left(1 - \frac{\sum_{l=1}^{i-1} R_{lj}^{t} + \frac{R_{ij}^{t}}{2}}{\sum_{l=1}^{R_{\mathrm{i}}} R_{lj}^{t}}\right) \tag{12}$$

This equation assumes that V_{m}^{t} remains constant with depth. As discussed in Deng and Zhou [11], this condition holds in the current model where the depth to radius ratio $L_{\mathrm{d}}/r_{\mathrm{e}}$ is greater than 5.

2.5 Fluid Flows and Settlements

Fluid flows occur between contiguous elements in the mesh. As an example, element *ij* and its contiguous elements are extracted and plotted in Figure 5. As per Esrig [24], three streams of flow occur between the elements: vertical hydraulic flow q_{z}, radial hydraulic flow q_{r}, and electroosmotic flow q_{e}. The rates of flow are governed by the vertical hydraulic conductivity,

k_z, the radial hydraulic conductivity, k_r, and the electroosmotic conductivity k_e. When $t = 0$, $\vec{k}_{z,ij} \perp \vec{k}_{r,ij}$. When $t > 0$, the central elements consolidate faster than the peripheral elements, and, as a result, the soil layer and the elements incline as illustrated in Figure 5. The vector $\vec{k}_{z,ij}$ acts at an angle of θ_{ij}^t from the initial vector $\vec{k}_{v,ij}$. As suggested by Harr [25], the permeability $k_{z,ij}^t$ is modified as

$$k_{z,ij}^t = \frac{k_{v,ij}^t}{\cos^2\theta_{ij}^t + \dfrac{\sin^2\theta_{ij}^t}{r_k}} \tag{13}$$

where r_k is the permeability ratio arising from the soil layer anisotropy and expressed as $r_k = k_r / k_v$, and the inclination angle θ_{ij}^t is expressed as:

$$\theta_{ij}^t = \tan^{-1}\left(\frac{z_{ij}^t - z_{(i-1)j}^t}{\Delta r_i}\right) \tag{14}$$

The equivalent hydraulic conductivity, $k_{zs,ij}^t$, between elements ij and $i(j+1)$ is determined as

$$k_{zs,ij}^t = \frac{k_{z,i(j+1)}^t k_{z,ij}^t \left(L_{i(j+1)}^t + L_{ij}^t\right)}{L_{i(j+1)}^t k_{z,ij}^t + L_{ij}^t k_{z,i(j+1)}^t} \tag{15}$$

Similarly, the equivalent hydraulic conductivity, $k_{rs,ij}^t$, between elements ij and $(i+1)j$ is

$$k_{rs,ij}^t = \frac{2 r_k k_{v,(i+1)j}^t k_{v,ij}^t}{k_{v,ij}^t + k_{v,(i+1)j}^t} \tag{16}$$

The equivalent electroosmotic conductivity, $k_{es,ij}^t$, between elements ij and $(i+1)j$ is

$$k_{es,ij}^t = \frac{2 k_{e,ij}^t k_{e,(i+1)j}^t}{k_{e,ij}^t + k_{e,(i+1)j}^t} \tag{17}$$

On the boundaries, the permeability coefficients are approximated to the coefficients of the contiguous elements, i.e., $k^t_{\mathrm{zs},iR_j} = k^t_{\mathrm{z},iR_j}$, $k^t_{\mathrm{zs},i0} = k^t_{\mathrm{z},i1}$, $k^t_{\mathrm{zs},0j} = k^t_{\mathrm{z},1j}$, $k^t_{\mathrm{zs},R_ij} = k^t_{\mathrm{z},R_ij}$, $k^t_{\mathrm{es},0j} = k^t_{\mathrm{e},1j}$, and $k^t_{\mathrm{es},R_ij} = k^t_{\mathrm{e},R_ij}$.

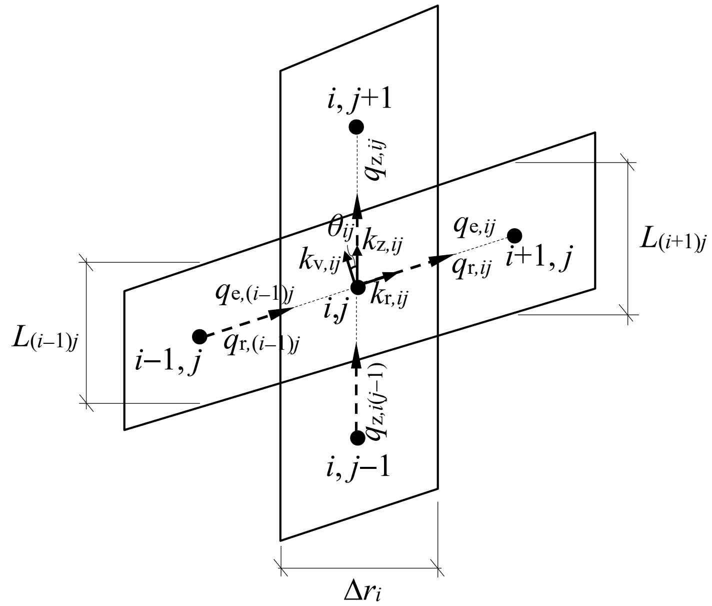

Figure 5 Fluid flows between individual elements.

At time step t, the rate of vertical flow, $q^t_{\mathrm{z},ij}$, between elements ij and $(i+1)j$ is equal to

$$q^t_{\mathrm{z},ij} = k^t_{\mathrm{zs},ij} i^t_{\mathrm{z},ij} 2\pi r_i \Delta r_i \tag{18}$$

where $i^t_{\mathrm{z},ij}$ is the hydraulic gradient between nodes ij and $i(j+1)$ and is equal to

$$i^t_{\mathrm{z},ij} = \frac{h^t_{i(j+1)} - h^t_{ij}}{z^t_{i(j+1)} - z^t_{ij}} \tag{19}$$

where the elevation z^t_{ij} is determined in terms of Eq. (2), and h^t_{ij}, the head at node ij, is equal to

$$h_{ij}^{t} = z_{ij}^{t} + \frac{u_{ij}^{t}}{\gamma_{\mathrm{w}}} \tag{20}$$

where the pore pressure u_{ij}^{t} is determined in terms of Eq. (9).

The rates of radial hydraulic flow, $q_{\mathrm{r},ij}^{t}$, and electroosmotic flow, $q_{\mathrm{e},ij}^{t}$, between elements ij and $i(j+1)$ are respectively equal to

$$q_{\mathrm{r},ij}^{t} = k_{\mathrm{rs},ij}^{t} i_{\mathrm{r},ij}^{t} 2\pi\left(r_i + \frac{\Delta r_i}{2}\right)\left(z_{\mathrm{c},ij}^{t} - z_{\mathrm{c},i(j-1)}^{t}\right)\sin\theta_{ij}^{t} \tag{21}$$

$$q_{\mathrm{e},ij}^{t} = k_{\mathrm{es},ij}^{t} i_{\mathrm{e},ij}^{t} 2\pi\left(r_i + \frac{\Delta r_i}{2}\right)\left(z_{\mathrm{c},ij}^{t} - z_{\mathrm{c},i(j-1)}^{t}\right)\sin\theta_{ij}^{t} \tag{22}$$

where $i_{\mathrm{r},ij}^{t}$ and $i_{\mathrm{e},ij}^{t}$ are the hydraulic gradient and voltage gradient between nodes ij and $(i+1)j$, respectively. The two gradients are expressed respectively as

$$i_{\mathrm{r},ij}^{t} = \frac{h_{(i+1)j}^{t} - h_{ij}^{t}}{\sqrt{\left(r_{i+1} - r_i\right)^2 + \left(z_{(i+1)j}^{t} - z_{ij}^{t}\right)^2}} \tag{23}$$

$$i_{\mathrm{e},ij}^{t} = \frac{V_{(i+1)j}^{t} - V_{ij}^{t}}{\sqrt{\left(r_{i+1} - r_i\right)^2 + \left(z_{(i+1)j}^{t} - z_{ij}^{t}\right)^2}} \tag{24}$$

At time step $t+\Delta t$ element ij consolidates. The element volume, $A_{ij}^{t+\Delta t}$, and void ratio, $e_{ij}^{t+\Delta t}$, are updated respectively as

$$A_{ij}^{t+\Delta t} = A_{ij}^{t} - \left(q_{\mathrm{e},ij}^{t} - q_{\mathrm{e},(i-1)j}^{t} + q_{\mathrm{r},ij}^{t} - q_{\mathrm{r},(i-1)j}^{t} + q_{\mathrm{z},ij}^{t} - q_{\mathrm{z},i(j-1)}^{t}\right)\Delta t \tag{25}$$

$$e_{ij}^{t+\Delta t} = \frac{A_{ij}^{t+\Delta t}\left(1 + e_{0,ij}\right)}{A_{0,ij}} - 1 \tag{26}$$

The settlement of column i, $S_{i}^{t+\Delta t}$, is expressed as

$$S_{ij}^{t+\Delta t} = H_0 - \frac{\left(z_{\mathrm{c},(i-1)R_\mathrm{j}}^{t+\Delta t} + z_{\mathrm{c},iR_\mathrm{j}}^{t+\Delta t}\right)}{2} \tag{27}$$

where $z_{\mathrm{c},(i-1)R_\mathrm{j}}^{t+\Delta t}$ and $z_{\mathrm{c},iR_\mathrm{j}}^{t+\Delta t}$ are obtained in terms of Eq. (3). For the soil layer, the average settlement, $S_{\mathrm{avg}}^{t+\Delta t}$, and the average degree of consolidation, $U^{t+\Delta t}$, are respectively expressed as

$$S_{\mathrm{avg}}^{t+\Delta t} = \frac{\sum_{i=1}^{R\mathrm{i}} \sum_{j=1}^{R\mathrm{j}} \left(A_{0,i} - A_{ij}^{t+\Delta t}\right)}{\pi\left(r_\mathrm{e}^2 - r_\mathrm{w}^2\right)} \tag{28}$$

$$U^{t+\Delta t} = \frac{S_{\mathrm{avg}}^{t+\Delta t}}{S} \tag{29}$$

where S is the final average settlement of the soil layer when all streams of flow reach equilibrium under the applied voltage, vacuum and surcharge load. The equilibrium is reached when two consecutive average settlements have a sufficiently small difference, i.e., on the order of 10^{-4} m.

2.6 Boundary Conditions

In Figure 3, if the bottom boundary is drained, the hydraulic gradient $i_{\mathrm{z},i0}^{t}$ is expressed as

$$i_{\mathrm{z},i0}^{t} = \frac{h_{i,1}^{t} - h_{\mathrm{wb}} + \dfrac{p_{i,\mathrm{b}}^{t}}{\gamma_\mathrm{w}}}{z_{i,1}^{t}} \tag{30}$$

where $p_{i,\mathrm{b}}^{t}$ is the vacuum pressure applied on the bottom boundary; otherwise, $i_{\mathrm{z},i0}^{t} = 0$. If the top boundary is drained, the hydraulic gradient $i_{\mathrm{z},iR_\mathrm{j}}^{t}$ is expressed as

$$i^t_{\mathrm{z},iR_\mathrm{j}} = \frac{2\left(h_{\mathrm{wt}} - \dfrac{p^t_{i,\mathrm{t}}}{\gamma_w} - h^t_{i,R_\mathrm{j}}\right)}{L^t_{i,R_\mathrm{j}} \sin\theta^t_{i,R_\mathrm{j}}} \tag{31}$$

where $p^t_{i,\mathrm{t}}$ is the vacuum pressure applied on the top boundary; otherwise, $i^t_{\mathrm{z},iR_\mathrm{j}} = 0$. At the cathode, the hydraulic gradient $i^t_{\mathrm{r},0j}$ and the voltage gradient $i^t_{\mathrm{e},0j}$, at an elevation $z_{1,j} \geq H_0 - L_\mathrm{d}$, are respectively expressed as

$$i^t_{\mathrm{r},0j} = \frac{h^t_{1,j} - \left(h_{\mathrm{wt}} - \dfrac{p^t_j}{\gamma_\mathrm{w}}\right)}{\sqrt{\left(\dfrac{\Delta r_1}{2}\right)^2 + \left(z^t_{1,j} - \dfrac{z^t_{\mathrm{c},0j} + z^t_{\mathrm{c},0(j-1)}}{2}\right)^2}} \tag{32}$$

$$i^t_{\mathrm{e},0j} = \frac{V_{1,j}}{\sqrt{\left(\dfrac{\Delta r_1}{2}\right)^2 + \left(z^t_{1,j} - \dfrac{z^t_{\mathrm{c},0j} + z^t_{\mathrm{c},0(j-1)}}{2}\right)^2}} \tag{33}$$

In addition, $i^t_{\mathrm{r},0j} = i^t_{\mathrm{e},0j} = 0$ at an elevation $z_{1,j} < H_0 - L_\mathrm{d}$. At the anodes, $i^t_{\mathrm{r},R_\mathrm{i}j} = i^t_{\mathrm{e},R_\mathrm{i}j} = 0$ for no drain.

2.7 Time Increment

The EC3 model adopts the criteria used in model EC2 [11] to determine the time increment Δt as:

$$\Delta t = \min\left\{ \begin{array}{c} \dfrac{\alpha\gamma_\mathrm{w} a^t_{\mathrm{v},ij} \left(L^t_{ij}\right)^2}{k^t_{\mathrm{v},ij}\left(1+e^t_{ij}\right)}, \quad \dfrac{\alpha\gamma_\mathrm{w} a^t_{\mathrm{v},ij} \left(\Delta r_i\right)^2}{k^t_{\mathrm{h},ij}\left(1+e^t_{ij}\right)}, \\ \left|\dfrac{0.001 A_{0,i}\left(e_{0,j} - e_{\mathrm{f},j}\right)}{\left(1+e_{0,j}\right)\left(q^t_{\mathrm{e},ij} - q^t_{\mathrm{e},(i-1)j} + q^t_{\mathrm{r},ij} - q^t_{\mathrm{r},(i-1)j} + q^t_{\mathrm{z},ij} - q^t_{\mathrm{z},i(j-1)}\right)}\right| \end{array} \right\} \tag{34}$$

where α is constant in the process of consolidation and is taken as 0.4. As per Deng and Zhou [11], the three criteria are defined to attain convergence in vertical hydraulic flow, horizontal hydraulic flow, and horizontal electroosmotic flow.

3 EC3 COMPUTER PROGRAM

The flow chart for the main algorithm is presented in Figure 6. At the initial phase, the required input data includes the number of the elements (R_i, R_j), the geometry of the soil layer (H_0, L, L_d, d_e), the initial vertical stress on the upper boundary (q_0), the effective stress increment (Δq_i^t), the voltage gradient (V_m^t), the vacuum load (p_j^t), the specific gravity of solids (G_s), the electrical resistivity of pore fluid (ρ_w) and solids (ρ_s), and the data points for the constitutive relationships, boundary conditions, and termination criteria for the program. The number of elements is determined in terms of the scale of the soil layer, the accuracy and computation time, and a general computer system suffices, as discussed in Zhou *et al.* [7]. According to the initial input data, EC3 computes the geometric properties for each element (L_0, Δr_i, z_{ij}, $z_{c,ij}$), the initial void ratio ($e_{0,ij}$) and the final void ratio ($e_{f,ij}$). When the effective stress increment (Δq_i^t), voltage (V_m^t) and vacuum loads (p_j^t) are applied to the soil layer, the program starts iterations using the corresponding time step increments. In each iteration, the pore pressure (u), effective stress (σ'), void ratio (e), electrical resistivity (ρ), coefficients of hydraulic permeability (k_h, k_z), and electroosmotic permeability (k_e) are calculated for each element in terms of the specified constitutive relationships. Meanwhile, the calculations give the following outputs: the rates of flow, the new heights of each element, the average settlements of the soil mass, and the local and average degrees of consolidation. Program execution terminates if $t > t_{final}$ or $\Delta S < m$ where t_{final} is a user-specified elapsed time and m is a sufficiently small value, i.e., $\times 10^{-4}$ m. When the value of m is reached, the program moves to an *e* value check: the final void ratio output ($e_{\mathrm{f1},ij}$) versus the final void ratio input ($e_{\mathrm{f},ij}$) for each element. If disagreement exists, $e_{\mathrm{f},ij}$ reads $e_{\mathrm{f1},ij}$, and the loop is executed another time. If the two void ratios agree, all streams of fluid flow have reached equilibrium, and the average settlement (S^{t}_{avg}) at this time is the final settlement (*S*). Given the final settlement, the average degree of consolidation (U^{t}) at any elapsed time *t* can be determined.

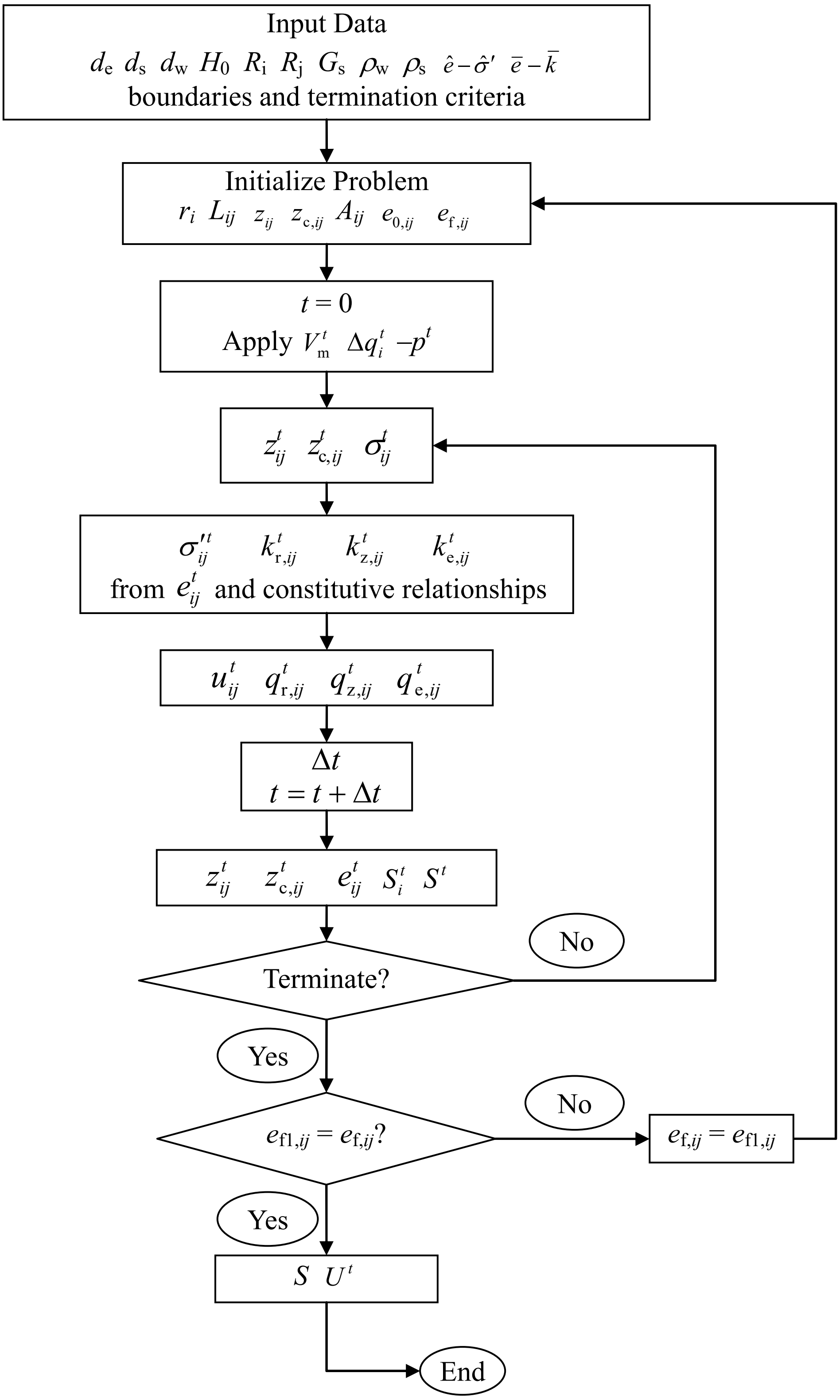

Figure 6 Flow chart for EC3 model

4 Model Validation

The performance of EC3 was validated in a laboratory test. The test was conducted in the apparatus shown in Figure 7. In the diagram, a cylindrical soil chamber (⌀500 × 250 mm in size) with a full-depth cathode sitting in the centre and an anode on the periphery of the soil is presented. The cathode was made of a round stainless-steel tube, ⌀15 × 250 mm, with 1 mm thick wall. The wall was perforated full-length with ⌀3 mm openings arranged in a triangular pattern with 10 mm at the centres. The cathode was wrapped with layers of non-weave fabrics as filters. The anode used 16 equally spaced stainless-steel rods each measuring ⌀4 × 250 mm. At the bottom of the cathode is an inlet that is fabricated to introduce the vacuum pressure from the pump. Between the inlet and the pump are the gas–liquid separator, pressure regulator, and scale, which were provided to gauge the pressure input and liquid output. Above the soil is the loading cap, similar in concept to the one for the oedometer test. We fabricated a small hole through the cap to enable wiring. The wiring transmits current from the power source to the electrodes. A dial gauge was mounted to the loading cap. The cap was rigid and can compress the soil evenly enabling the dial gauge to record the average soil settlement. On the periphery of the chamber, layers of membranes were used to seal the soil chamber to prevent vacuum loss.

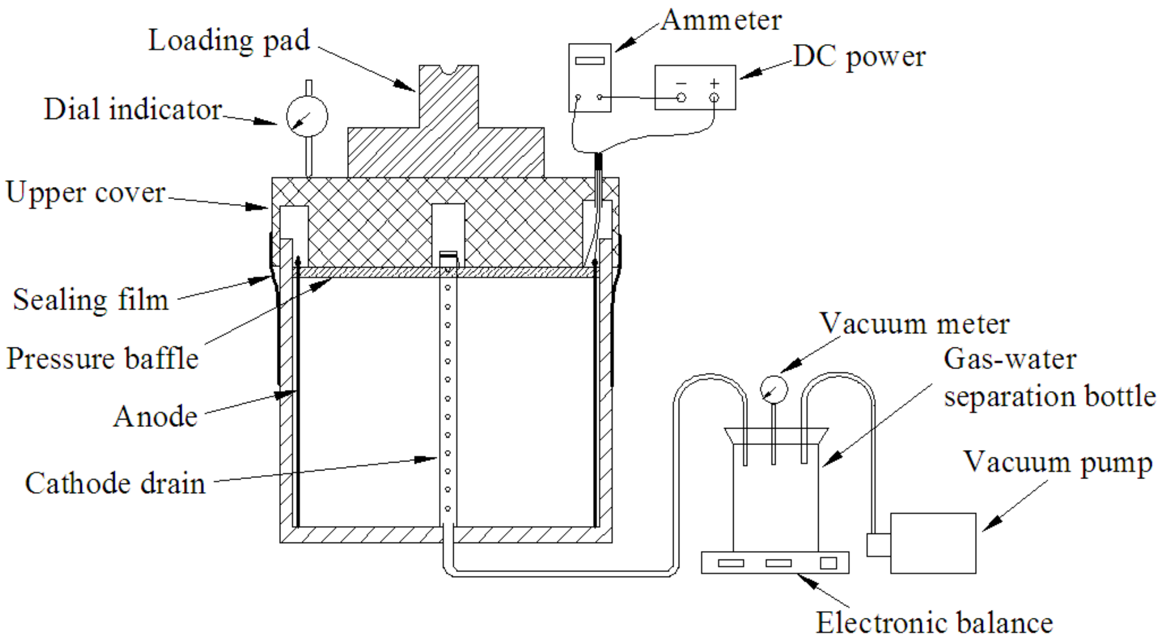

Figure 7 Schematic of electroosmosis–vacuum–surcharge preloading consolidation model.

We examined two test scenarios: electroosmosis−surcharge preloading and electroosmosis−vacuum preloading. The scenario of the electroosmosis−vacuum−surcharge preloading was not applied since the upper cover was not fabricated as expected to work towards the concurrent applications of surcharge and vacuum. The two tested scenarios, however, include all elements of the preloading processes and are able to cross check the performance of model EC3. The material used in the tests was a remoulded kaolinite that was the same as in the previous study [7]. The kaolinite was loaded in an effort to produce a saturated, uniform soil layer. The soil properties, load details and EC3 model parameters are provided in Table 1. In the test of electroosmosis–surcharge preloading, the voltage was 20 V enabling a voltage gradient of i_e= 170 V/m. The surcharge loads were applied incrementally in three stages, t = 0, 24 and 48 hours, to further examine the capability of the model in stepped loading conditions. In the test of electroosmosis–vacuum preloading, the voltage gradient remained the same. A vacuum pressure of –80 kPa was applied throughout. The pressure was assumed to remain constant in the cathode drain due to the relatively shallow depth of the drain. For the soil in the chamber, model EC3 created a mesh of 50×50 at a radial cross-section. The boundaries were set as drained cathode and closed anode.

Table 1 Test soil layer properties and model input values.

	Value used in two consolidation tests	
Property	Electroosmosis–surcharge preloading	Electroosmosis–vacuum preloading
Soil thickness H_0 (cm)	22.5	22.5
Specific gravity of solids G_s	2.62	2.62
Initial water content w_0	59.4%	59.7%
Initial void ratio e_0	1.57	1.57
Coefficient of compressibility C_c	0.22	0.22
Initial permeability coefficient k_{v0} (m/s)	2.1×10^{-9}	2.1×10^{-9}
Permeability parameter C_k	0.99	0.99
Permeability ratio r_k	1	1
Initial electroosmotic conductivity k_{e0} ($m^2 \cdot V^{-1} \cdot s^{-1}$)	5.3×10^{-9}	5.3×10^{-9}
Exponent for electroosmotic conductivity a	3.5	3.5
Electrical resistivity of solids ρ_s (Ω·m)	608	608
Electrical resistivity of pore fluid ρ_w (Ω·m)	4.5	4.5
Voltage V_m^t (V)	20	20
Load increment Δq_i^t (kPa)	12.5, 25 and 50 in stages	N/A

Vacuum pressure p_j^t (kPa)	N/A	–80
Model mesh (R_{i}, R_{j})	(50, 50)	(50, 50)
Diameter of influence zone d_e (cm)	25	25
Equivalent drain diameter d_w (cm)	1.5	1.5
Boundary conditions	Open cathode, closed anode	Open cathode, closed anode

The test and simulation results for the two scenarios are presented in Figure 8 and Figure 9. In Figure 8, the results include the settlement versus elapsed time for the soil layer subjected to the combined usage of voltage and surcharge loads. An up to 50 mm settlement (i.e., 22.2% strain) occurred, producing a large-deformation case. Excellent agreement was attained between the test and simulation results. The model even satisfactorily captured the jumps associated with the stepped loading. Similarly, excellent agreement was attained in Figure 9, which presents the water discharge versus elapsed time for the test of electroosmosis–vacuum preloading. In this test, the water discharge was a preferred measure of the consolidation since it was the water flow that governed the consolidation process. Given the results agreement in the two tests, the capability of model EC3 in simulating large-deformation consolidation is validated.

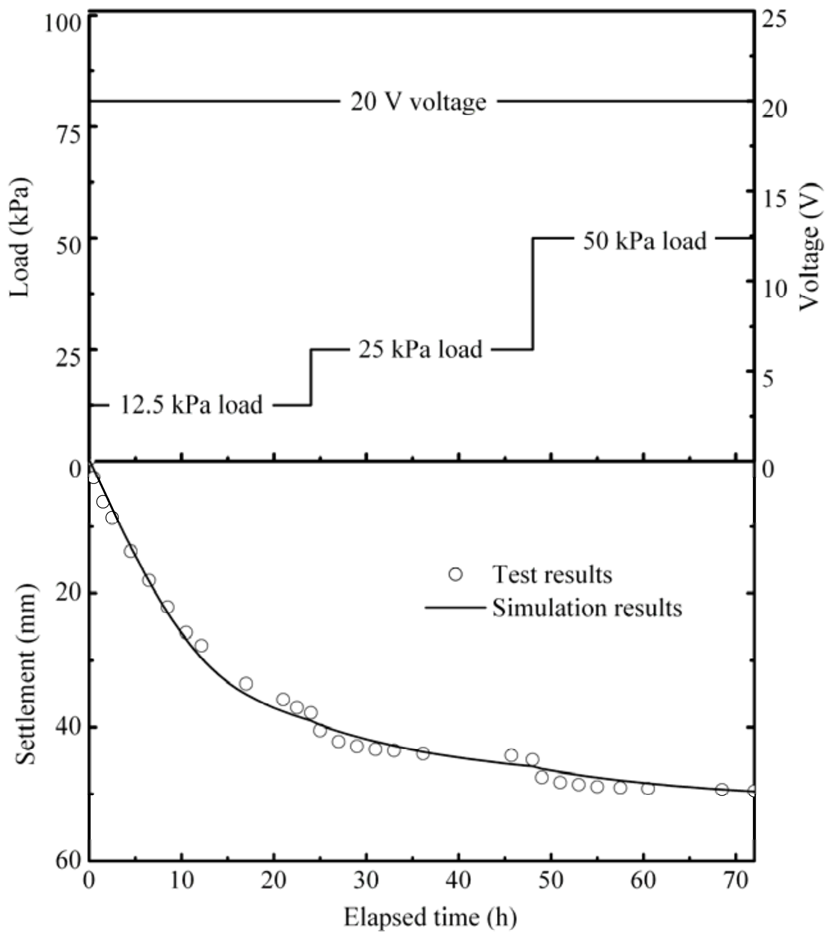

Figure 8 Settlement versus elapsed time for the soil layer subjected to electroosmosis–surcharge preloading where constant voltage and stepped surcharge were applied.

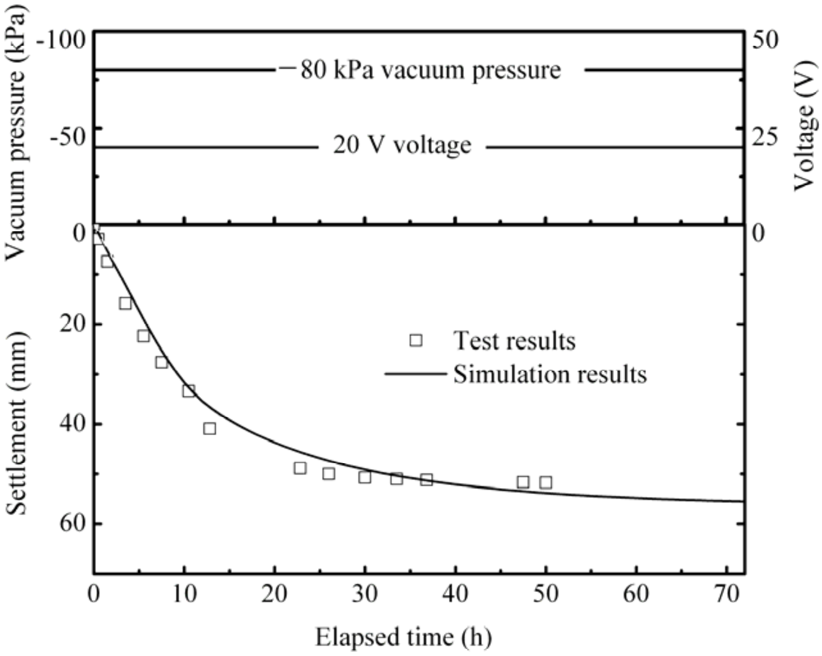

Figure 9 Water discharge versus elapsed time for the soil layer subjected to electroosmosis–vacuum preloading where constant voltage and constant vacuum pressure were applied.

5 Simulation Results

Simulations were performed to optimise the consolidation process. The optimisation aims were the following: *i*) accelerating consolidation at an optimised power load, *ii*) assessing the influence of a smear zone on the consolidation results, and *iii*) further examining the effect of varying properties of the smear zone on the consolidation results. To attain these aims, five cases were designed as presented in Table 2. The five cases vary in consolidation efforts: the voltage is V_{m}^{t}=0, 20 or 30 V, the vacuum pressure is p_{j}^{t}=0, –50 or –80 kPa, and the load increment is Δq_{i}^{t}=0, 60 or 100 kPa. Specifically, for cases 1−3, one preloading element was not applied, and these were designed as the tests. Case 4, which applied all three of the elements at the corresponding levels applied in cases 1−3, was designed as the benchmark, and case 5 acted as an additional benchmark test that used a set of lower loads than in case 4.

All cases were applied to the model presented in Figure 3. The model conditions are presented in Table 3. In the table, the soil properties were attained from Deng and Zhou [6] and Zhou *et al.* [7]. The ground and PVD installations were determined in terms of field applications. The value ranges used in the table define a medium thick, saturated, high compressibility clay layer.

Table 2 Simulation cases examined to optimise consolidation process.

Case	Consolidation process	Voltage V (V)	Vacuum p (kPa)	Load Δq (kPa)
1	Vacuum–surcharge	0	–80	100
2	Electroosmosis–surcharge	30	0	100
3	Electroosmosis–vacuum	30	–80	0
4	Electroosmosis–vacuum–surcharge	30	–80	100
5	Electroosmosis–vacuum–surcharge	20	–50	60

Table 3 Soil layer properties and model input values.

Property	Value
Soil layer thickness H_0 (m)	5
Electrode installation depth L_d (m)	5
PVD equivalent diameter d_w (m)	0.05
Diameter of influence zone d_e (m)	2
Specific gravity of solids G_s	2.65
Electrical conductivity of water ρ_w (Ω·m)	10
Electrical conductivity of solids ρ_s (Ω·m)	1,000
Coefficient of compressibility C_c	1.0

Permeability parameter C_k	1.0
Exponent for electroosmotic conductivity a	3.5
Initial void ratio e_0	2.1
Initial permeability coefficient k_{v0} (m/s)	4.0×10^{-9}
Initial electroosmotic conductivity k_{e0} ($m^2 \cdot V^{-1} \cdot s^{-1}$)	2.0×10^{-9}
Permeability ratio r_k	1.5
Initial surcharge preloading q_0 (kPa)	50
Boundary conditions	Upper: open, lower: closed
Model mesh (R_i, R_j)	(51, 51)

5.1 Consolidation optimisation

The simulation results for cases 1–4 are provided in Figure 10. The results present pore pressure isochrones captured for elements (i, 25) (i.e., the mid-depth) at three elapsed times: 10, 100 and 300 days. At day 10 (Figure 10 (a)), the pore pressures for cases 1 and 4 remain at approximately 100 kPa across the electrodes, except in the proximity of the cathode where the pore pressures drop to −80 kPa. The value of 100 kPa agrees with the load increment applied to the three cases, and the pressure of −80 kPa echoes the vacuum applied on the PVD. The gradients remain at a similar slope for cases 1 and 4. A similar isochrone occurs in case 2, except for the pressure at the cathode, which is zero. The zero pore-pressure zero-pore pressure echoes the drained boundary at the cathode as well as the lack of vacuum element. The pore pressures for case 3 are as low as zero across the electrodes, except in the proximity of the cathode. The value of zero for the pressure arises from the lack of the element of load increment for this case. Although the electric field is applied, the field does not build to a positive pressure, which agrees with the nature of electroosmosis as per Casagrande [26] and Esrig [24]. In all of the four cases, the zones where the pressure gradients occur coincide in the 0 to 0.2 m zones surrounding the PVD. It is noteworthy that, although case 4 acts as the benchmark and applies all three elements of the processes, the pore pressures at day 10 for this case do not vary noticeably from those of case 1. This means that at day 10, or the early-stage of consolidation, the voltage or electric field does not work towards the pore pressure development as much as attained in the other two elements of the process (i.e., vacuum and surcharge preloading). Conversely, the lack of either of these two elements influences the pressure isochrones, at least at day 10.

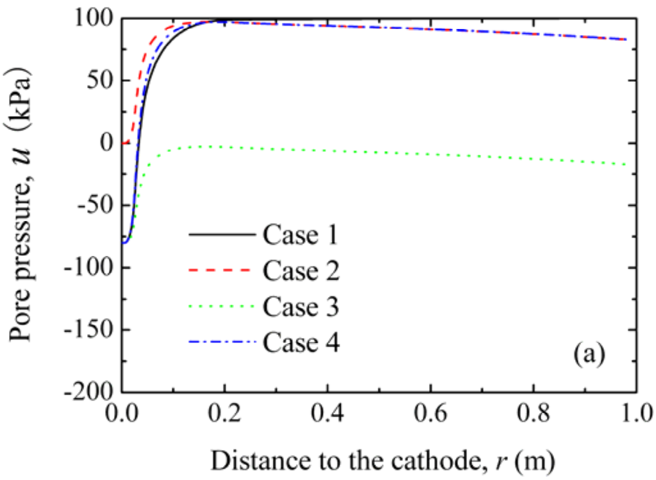

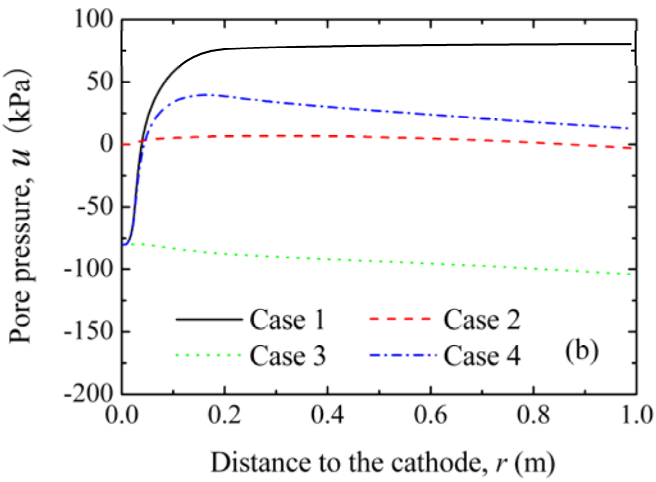

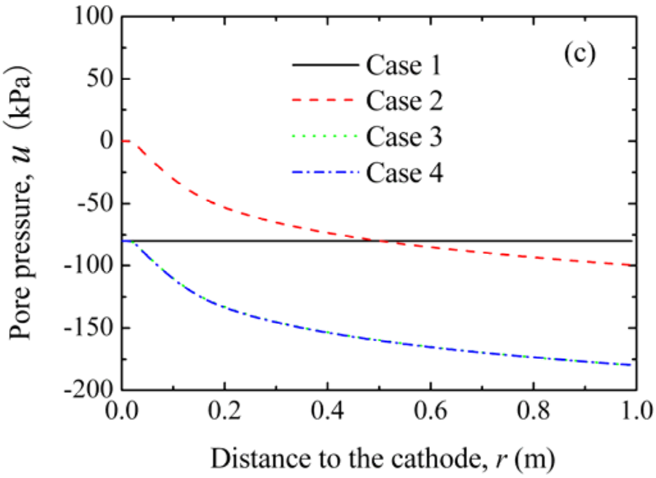

Figure 10 Pore pressure isochrones of the soil layer subjected to case 1 electroosmosis–surcharge preloading, case 2 electroosmosis–surcharge preloading, case 3 electroosmosis–vacuum preloading, and case 4 electroosmosis–vacuum–surcharge preloading, captured at the elapsed times: (a) 10 d, (b) 100 d, and (c) 300 d.

When time elapsed to day 100, the pore pressure isochrones moved apart, and the pressures dissipated at different rates. The pressures for case 4 dissipate at a rate greater than in case 1, albeit their isochrones coincide at day 10. Case 4 attains a pressure of 20–30 kPa for the locations of 0.2 m and beyond. On the same locations, case 1 maintains pressures of 75 kPa or so. The difference in the dissipation rate demonstrates the capacity of the element of electroosmosis in accelerating water discharge and thus the drop in the positive pore pressure at the mid–late stage of consolidation. Similarly, quick dissipation rates occur in cases 2 and 3. In case 2, where the electroosmosis and surcharge preloading are combined, the pore pressures fade off to nearly zero. In case 3, which combines electroosmosis and vacuum, the pore pressures become negative and have a range of –80 to –100 kPa. In both cases, the element of electroosmosis contributes to a great extent to the dissipation of positive pressures and the development of negative pressures.

When the time further elapses to day 300, the pressure dissipations move into equilibrium and the isochrones become constant. For case 1 (i.e., the vacuum–surcharge case), the pore pressures remain at –80 kPa throughout the electrodes' space agreeing with the assumed condition of constant vacuum pressure distribution. The isochrones for cases 3 and 4 coincide developing from –80 kPa at the cathode to –180 kPa at the anode. As per Esrig [24], the negative pressures are comprised of two components: the pressures arising from the application of the –80 kPa vacuum and the pressure caused by the electroosmotic process. The two components are represented by the isochrones for cases 2 and 3. From the four isochrones, it is suggested that the pressures arising from the surcharge preloading are positive and are able to dissipate (to zero) over time. The pressures from the electroosmosis or vacuum are negative and eventually grow to constant values when the consolidation reaches equilibrium. The negative pressures likely dissipate if the consolidation process (i.e., electroosmosis or vacuum) ceases, as discussed in Deng and Zhou (2016).

The average settlement and degree of consolidation for the soil layer that is examined are presented in Figure 11. The results are plotted over the elapsed time for the five cases. Cases 1, 2 and 3, where two elements of the preloading processes are applied, attain average settlements of 1.06, 1.08 and 1.02 m, respectively. These settlements correspond to 21.2%, 21.5% and 20.4% settlement rates for the 5 m deep soil layer. The agreement in the settlement rates suggests that the two-element combined processes, independent of the combinations, yields similar final settlement values for the input values examined in this study. Case 4, which applies the three preloading elements, attains a settlement of 1.29 m, i.e., a settlement rate of 25.8%. The rate is approximately 5% greater than the results obtained in cases 1–3. It is suggested that the three-element combined process outperforms in final settlement the two-element combined processes when the corresponding input values remain the same. In case 5, where the input values are reduced by 30–40%, the final settlement is

1.02 m. The value falls into the range of attained values in cases 1–3. This equivalence represents a trade-off between the following: *i*) the choices of preloading elements that are applied, *ii*) the input values for the elements, and *iii*) the time to attain a desirable settlement. Specifically, the three-element process (case 4) using a set of lower energy inputs is able to attain similar settlements to those attained by the two-element processes (cases 1–3), which use a set of higher energy inputs. Meanwhile, case 4 expends the least amount of time attaining a specific settlement. This offers a direction for optimisation of consolidation where the energy and time are considered. The time that is required to attain a degree of consolidation is another factor to consider. In Figure 11, the sequence for the degree of consolidation in descending order, at any elapsed time, is cases 3, 2, 5, 4 and 1. For example, at day 100, the degrees of consolidation are 74% for case 3, 70.5% for case 2, 61% for case 5, 60% for case 4 and 47% for case 1. Case 1 takes more time than the rest of the scenarios to attain the same degree of consolidation.

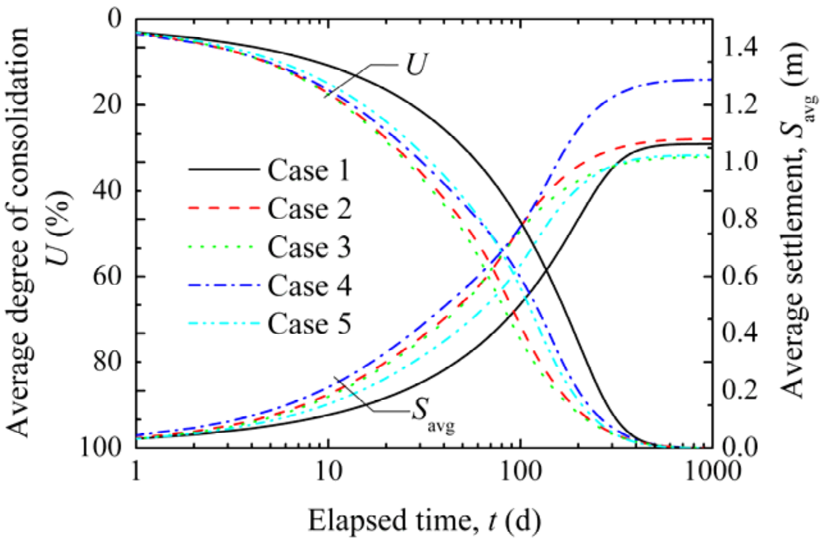

Figure 11 Average settlement and average degree of consolidation versus elapsed time for the soil layer subjected to case 1 electroosmosis–surcharge preloading, case 2 electroosmosis–surcharge preloading, case 3 electroosmosis–vacuum preloading, and cases 4 and 5

electroosmosis–vacuum–surcharge preloading, at varying preloading input values.

5.2 Influence arising from smear zone

To gain a further insight into the consolidation efficiency, the influence of the smear zone on consolidation was examined. For cases 1–4, a smear zone was developed surrounding the PVD, as presented in Figure 3. The smear zone has a diameter of d_s=0.2 m and a permeability coefficient of k_{sr}=0.5k_r. The rest of the conditions remain the same as for cases 1–4, as provided in Table 2 and Table 3. The average settlement results are presented in Figure 12. In the figure, the settlement curves for cases 1–4 are influenced by the presence of the smear zone. The levels of influence, however, are different among the cases. Case 1 shows the most noticeable influence; the smear zone delays the settlement from day 10 to the late stage of consolidation. For cases 2–4, marginal influences on the settlement are identified. Meanwhile, for these three cases, the presence of smear zones led to greater final settlements, i.e., a further 0.1–0.2 m settlement. The additional settlement arises from the lower permeability of the smear zone which, as per Esrig [24], requires a longer amount of time for the electroosmosis and greater consolidation to reach equilibrium of the flows.

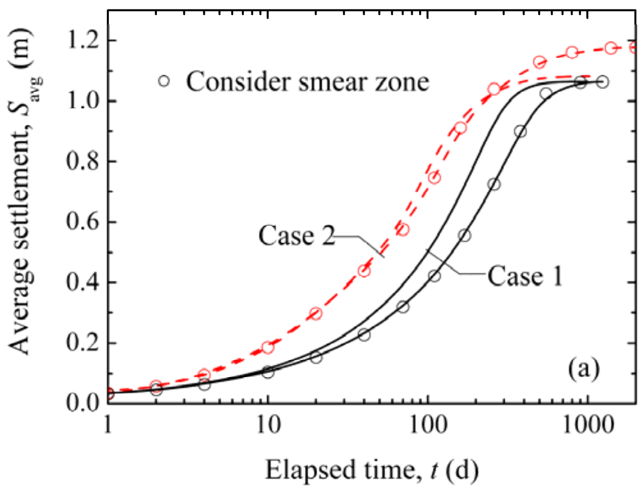

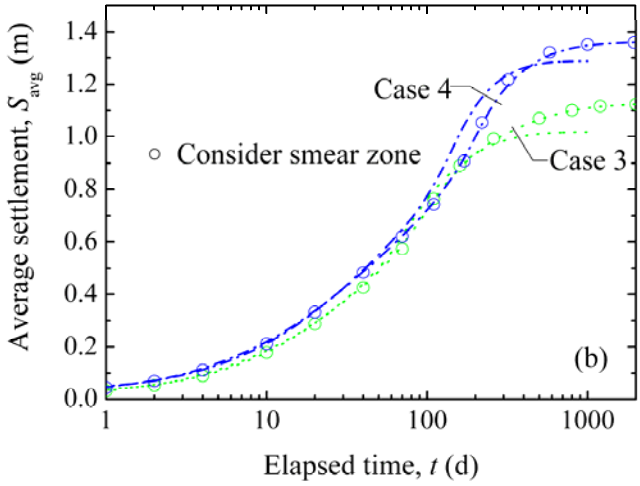

Figure 12 Average settlements versus elapsed time for the soil layer subjected to: (a) case 1 electroosmosis–surcharge preloading, case 2 electroosmosis–surcharge preloading; (b) case 3 electroosmosis–vacuum preloading, and case 4 electroosmosis−vacuum−surcharge preloading, with or without the presence of smear zone.

A similar influence occurs on the average degree of consolidation, as presented in Figure 13. The presence of a smear zone tends to delay the progress of consolidation for all cases; from day 20 for cases 1–3 and day 30 for case 4. The delays extend and become more noticeable after 100 days and, at the end of the consolidation, tend to fade off. The delays arise from the lower permeability of the smear zone, which reduces the water flow and consolidation. This means that the presence of a smear zone is able to influence the consolidation degree in spite of the choices of the preloading elements applied to the soil layer. The delays, however, may vary depending on the permeability and thickness identified for the smear zones. Therefore, the goal for an efficient early- to mid-stage consolidation is to reduce the disturbance occurring at the smear zone.

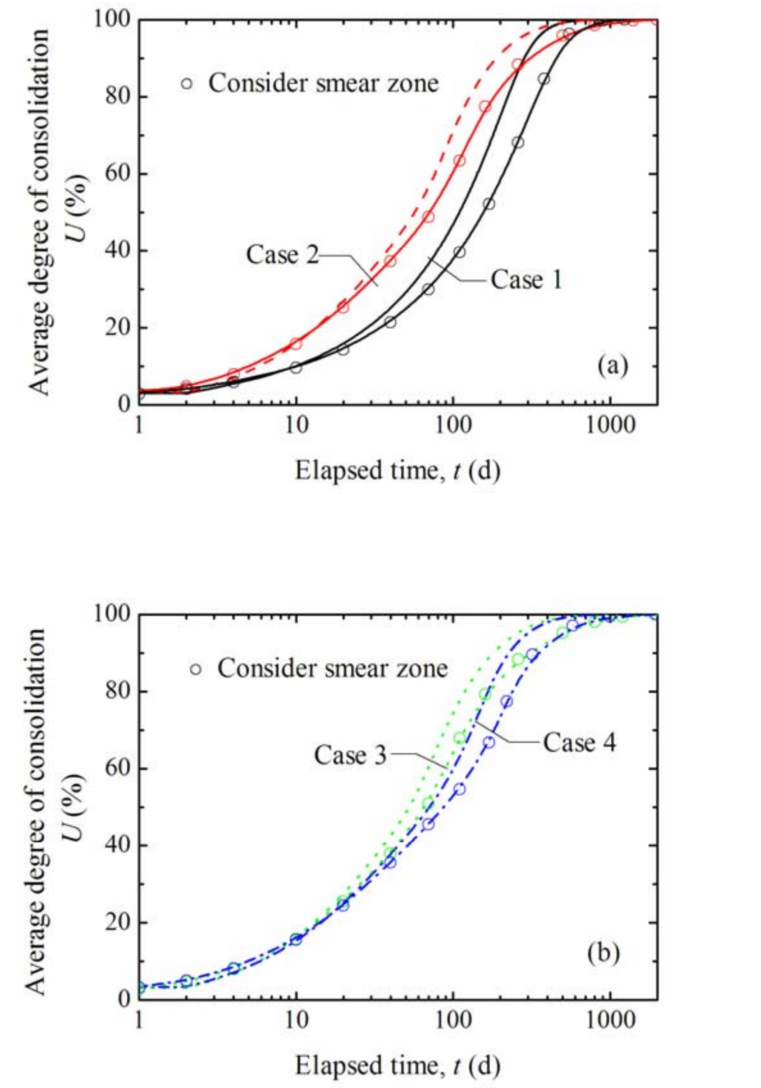

Figure 13 Average degree of consolidation versus elapsed time for the soil layer subjected to: (a) case 1 electroosmosis–surcharge preloading, case 2 electroosmosis–surcharge preloading; (b) case 3 electroosmosis–vacuum preloading, and case 4 electroosmosis–vacuum–surcharge preloading, with or without the presence of a smear zone.

5.3 Effect of varying properties of the smear zone

A smear zone varies in diameter and permeability depending on the mandrel size and soil type. The normal ranges are up to four times the drain diameter and as low as one half of the native soil permeability [27, 28]). Therefore, these ranges are considered in the design of two parameter studies for the smear zone: *i*) the permeability is $k_{sr} = 0.5k_r$, and the diameter varies as d_s/d_w =0, 2, 4, and 8; *ii*) the diameter is d_s = 0.2 m, and the permeability varies as k_{sr}/k_r =1, 0.5 and 0.2. The two data sets were applied to the benchmark case 4 presented in Table 2. The rest of the inputs remain the same as in Table 3. It is noted that the input d_s/d_w =0 or k_{sr}/k_r =1 represents the case where there is no smear zone. The simulation results are provided in Figure 14. In Figure 14(a), the average settlement increases marginally with the smear zone diameter where the soils permeability remains the same. The corresponding settlement values are 1.29, 1.32, 1.36 and 1.4 m. The curves of the degree of consolidation for the three smeared cases remain close and independent of the diameter variation. These curves, however, develop in a pattern that is distinct from that for the no-smear case. The relationships in curve development suggest that a thin smear zone causes a similar difference in the degree of consolidation as thick zones. In Figure 14(b), the average settlement increases with the decrease in the smear zone permeability where the smear zone diameter is fixed. The settlement values are 1.29, 1.36 and 1.52 m. At the same time, the less permeable the smear zone is, the less the degree of consolidation in the soil layer. These results mean that the permeability of the smear zone inversely influences the layer settlement and positively influences the degree of consolidation if the other conditions remain the same.

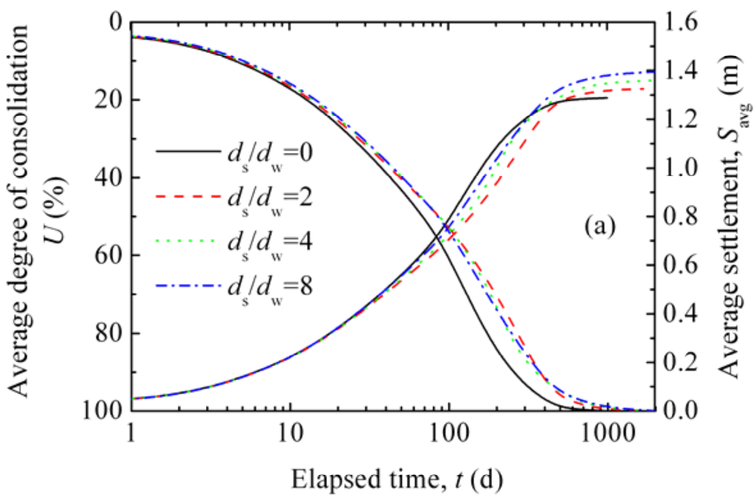

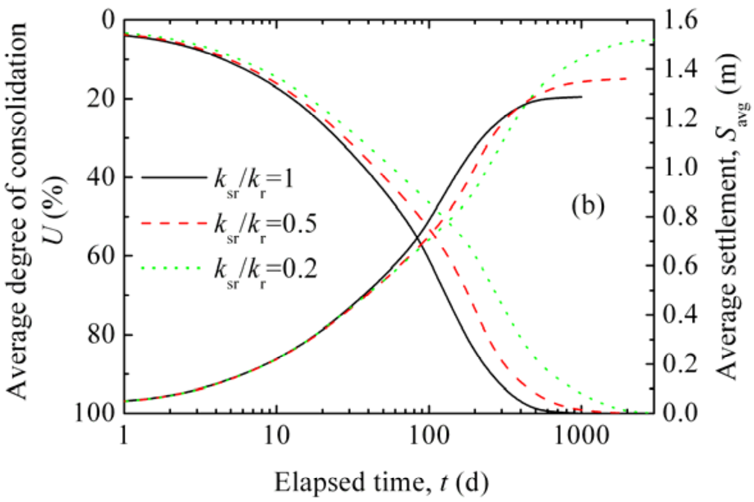

Figure 14 Average settlement and average degree of consolidation versus elapsed time for the soil layer subjected to combined electroosmosis–vacuum–surcharge preloading process: (a) effect of smear zone diameter, and (b) effect of smear zone permeability.

6 Conclusions

EC3 is a numerical model for the consolidation of a soil layer that is subjected to the combined electroosmosis–vacuum–surcharge preloading process. The model develops an algorithm of 3D radial consolidation and considers electroosmosis, hydraulic permeation, radial electric field, soil self-weight, and general constitutive relationships. The algorithm also accounts for the nonlinear changes in physical soil properties, time-dependent loading, and vacuum and electric density acting at the boundaries of the soil layer.

EC3 provides the following quantities as a function of time: *a*) rate of flow at the boundaries and *b*) degree of consolidation of the soil layer. EC3 provides the following quantities as a function of time and location within the soil layer: *a*) settlement, *b*) void ratio, *c*) pore pressure, *d*) vertical effective stress, *e*) moisture content, and *f*) electric potential and current density.

EC3 was validated through laboratory tests and applied to simulation studies. The simulation results suggest that: *a*) the three-element process attains the final settlement approximately 5% greater than those attained by the two-element processes, where the corresponding input values remain the same; *b*) using lower energy inputs, the three-element process is able to attain similar consolidation results as the two-element processes do; and *c*) the presence of a smear zone delays the progress of consolidation and increases the final settlement.

EC3 assumes a fully saturated soil condition in the consolidation process, enabling Darcy fluid flow. Depending on the boundaries of the scenarios, this condition may not stand in the late stage of consolidation. This limitation can be eliminated by introducing concepts for unsaturated soils into the model in future development.

Notations

The following symbols are used in this paper:

A Element volume

A_{ij} Volume of element *ij*

a_v Coefficient of compressibility

C_c Compression index

C_k Hydraulic permeability index

d_e Diameter of influence zone

d_s Smear zone equivalent diameter

d_w PVD equivalent diameter

e Void ratio

e_0 Initial void ratio

$e_{f,ij}$ Final void ratio input for element *ij*

$e_{f1,ij}$	Final void ratio output for element *ij*
G_s	Specific gravity of soil solids
h_{ij}	Head of element *ij*
h_{wt}	Head at top boundary
h_{wb}	Head at bottom boundary
H_0	Initial thickness of soil layer
i	Element radial coordinate
i_e	Voltage gradient, electric potential gradient
$i_{e,ij}$	Voltage gradient between elements *ij* and (*i*+1)*j*
i_r	Radial hydraulic gradient
$i_{r,ij}$	Radial hydraulic gradient between elements *ij* and (*i*+1)*j*
is	Vertical hydraulic gradient
$is_{,ij}$	Vertical hydraulic gradient between elements *ij* and *i*(*j*+1)
j	Element vertical coordinate
k	Coefficient of hydraulic (or electroosmotic) permeability
k_e	Coefficient of electroosmotic permeability
k_{e0}	Coefficient of initial electroosmotic permeability
$k_{es,ij}$	Equivalent series coefficient of electroosmotic permeability between elements *ij* and (*i*+1)*j*
k_h	Hydraulic conductivity
k_r	Radial hydraulic conductivity
$k_{rs,ij}$	Equivalent series radial hydraulic conductivity between elements *ij* and (*i*+1)*j*
k_{sr}	Smear zone radial hydraulic conductivity
k_v	Vertical hydraulic conductivity
k_z	Amended coefficient of vertical hydraulic permeability

$k_{zs,ij}$ Equivalent series vertical hydraulic conductivity between elements ij and $i(j+1)$

L_d PVD penetration length

L_{ij} Average height of element ij

L_0 Initial height of element ij

m Small number of settlement difference

p Vacuum load

p_t Vacuum load at top boundary

p_b Vacuum load at lower boundary

q Rate of flow

q_0 Initial overburden effective stress at top boundary

$q_{z,ij}$ Rate of hydraulic flow between elements ij and $i(j+1)$

$q_{r,ij}$ Rate of hydraulic flow between elements ij and $(i+1)j$

$q_{e,ij}$ Rate of electroosmotic flow between elements ij and $(i+1)j$

r Radial coordinate

r_e Radius of influence zone

r_k Factor of ratio for hydraulic permeability

r_s Smear zone equivalent radius

r_w PVD equivalent radius

R Electrical resistance

R_i Number of elements in radial dimension

R_j Number of elements in vertical dimension

R_m Number of data points for compressibility curve

R_n Number of data points for permeability curves

S_{avg} Average settlement of soil layer

S_i Settlement of column i

S	Final average settlement of soil layer
t	Elapsed time of consolidation
t_{final}	Final elapsed time of consolidation
u	Pore pressure
U	Average degree of consolidation
V	Electric potential difference
V_{ij}	Electric potential at element *ij*
V_{m}	Effective voltage
w_0	Initial water content
z	Vertical coordinate
$z_{\mathrm{c},ij}$	Elevation of upper corner of element *ij*
z_{ij}	Elevation of node of element *ij*
α	Constant used to determine the time step increment
γ	Saturated unit weight of soil
γ_{w}	Unit weight of water
θ	Angle of inclination of element
ρ	Electrical resistivity
ρ_{s}	Electrical resistivity of soil solids
ρ_{w}	Electrical resistivity of pore fluid
σ	Total vertical stress
σ'	Effective vertical stress
Δe	Change in void ratio
Δq	Load increment
Δr_i	Radial width of element *i*

Δt Time step increment

Superscripts

a Exponent used to determine the electroosmotic permeability

m mth data point for compressibility curve

n nth data point for permeability curve

t Elapsed time of consolidation

^ data points for compressibility curve

¯ data points for permeability curves

Subscripts

i ith element in radial dimension

j jth element in vertical dimension

Acknowledgements

This study was supported by the National Natural Science Foundation of China (51608351) and the Natural Science Foundation of Tianjin (18JCYBJC22600).

References

[1] Griffin H, O'kelly BC. Ground improvement by vacuum consolidation-a review. Proceedings of the Institution of Civil Engineers: Ground Improvement. 2014;167(4):274-90.

[2] Xu B, Si W. Surcharge preloading consolidation analysis of coastal road considering permeability of dredged soil. IOP Conference Series: Earth and Environmental Science. 1 ed2017.

[3] Wang J, Ma JJ, Liu FY, Mi W, Cai YQ, Fu HT, et al. Experimental study on the improvement of marine clay slurry by electroosmosis-vacuum preloading. Geotext Geomembranes. 2016;44(4):615–22.

[4] Shi L, Wang QQ, Xu SL, Pan XD, Sun HL, Cai YQ. Numerical study on clogging of prefabricated vertical drain in slurry under vacuum loading. Granul Matter. 2018;20(4):74.

[5] Rujikiatkmajorn C. Physical modelling of soft clay consolidation using vacuum-surcharge method. Aust Geomech J. 2012;47(3):27–34.

[6] Deng A, Zhou YD. Modeling Electroosmosis and Surcharge Preloading Consolidation. II: Validation and Simulation Results. J Geotech Geoenviron. 2016;142(4):04015094.

[7] Zhou YD, Deng A, Wang C. Finite-difference model for one-dimensional electro-osmotic consolidation. Comput Geotech. 2013;54(152–65.

[8] Liu HL, Cui YL, Shen Y, Ding XM. A new method of combination of electroosmosis, vacuum and surcharge preloading for soft ground improvement. China Ocean Eng. 2014;28(4):511–28.

[9] Sun ZH, Gao MJ, Yu XJ. Vacuum preloading combined with electro-osmotic dewatering of dredger fill using electric vertical drains. Dry Technol. 2015;33(7):847–53.

[10] Liu HL, Cui YL, Shen Y, Ding XM. A new method of combination of electroosmosis, vacuum and surcharge preloading for soft ground improvement. China Ocean Eng. 2014;28(4):511-28.

[11] Deng A, Zhou YD. Modeling Electroosmosis and Surcharge Preloading Consolidation. I: Model Formulation. J Geotech Geoenviron. 2016;142(4):04015093.

[12] Wan TY, Mitchell JK. Electro-osmotic consolidation of soils. J Geotech Eng Div. 1976;102(5):473–91.

[13] Shang JQ. Electroosmosis-enhanced preloading consolidation via vertical drains. Can Geotech J. 1998;35(3):491–9.

[14] Hu L, Wu W, Wu H. Numerical model of electro-osmotic consolidation in clay. Geotechnique. 2012;62(6):537–41.

[15] Kianfar K, Indraratna B, Rujikiatkamjorn C. Radial consolidation model incorporating the effects of vacuum preloading and non-Darcian flow. Geotechnique. 2013;63(12):1060–73.

[16] Vu VT, Yang YY. Numerical modelling of soft ground improvement by vacuum preloading considering the varying coefficient of permeability. Int J Geotech Eng. 2018;12(3):258–66.

[17] Wu H, Hu LM. Numerical model of soft ground improvement by vertical drain combined with vacuum preloading. J Cent South Univ. 2013;20(7):2066–71.

[18] Deng A, Zhang M. A consolidation model of single drain driven by combiningvacuum preloadingand electroosmosis. GA 2012 - 5th Asian Regional Conference on Geosynthetics: Geosynthetics for Sustainable Adaptation to Climate Change2012. p. 191–200.

[19] Wu H, Hu L. Theoretical analysis and numerical simulation of vacuum preloading in combination with electro-osmosis consolidation. Geotechnical Special Publication. 211 GSP ed2011. p. 605–15.

[20] Townsend FC, Mcvay MC. SOA: Large Strain Consolidation Predictions. J Geotech Eng-ASCE. 1990;116(2):222–43.

[21] Feldkamp JR. Numerical-analysis of one-dimensional nonlinear large-strain consolidation by the finite-element method. Transport Porous Med. 1989;4(3):239–57.

[22] Yuan J, Hicks MA. Large deformation elastic electro-osmosis consolidation of clays. Comput Geotech. 2013;54(60–8.

[23] Fox PJ, Di Nicola M, Quigley DW. Piecewise-linear model for large strain radial consolidation. J Geotech Geoenviron. 2003;129(10):940–50.

[24] Esrig MI. Pore pressure, consolidation and electrokinetics. J Soil Mech Found Div. 1968;94(SM4):899–922.

[25] Harr ME. Groundwater and Seepage. New York: McGraw–Hill, 1962.

[26] Casagrande L. Electro-osmosis in soils. Geotechnique. 1949;1(3):159–77.

[27] Hansbo S. Consolidation by vertical drains. Geotechnique. 1981;31(1):45-66.

[28] Sathananthan I, Indraratna B. Laboratory evaluation of smear zone and correlation between permeability and moisture content. J Geotech Geoenviron. 2006;132(7):942-5.